Research Square

Preprints are preliminary reports that have not undergone peer review.
They should not be considered conclusive, used to inform clinical practice,
or referenced by the media as validated information.

Anode material and carbon powder-amended sludge immobilization jointly govern bioelectrochemical performance of Chlorella vulgaris- fed microbial fuel cells

Akhila U
Cochin University of Science and Technology
Md Tabish Noori
tnoori@unav.es
Universidad de Navarra
Rajesh PP
Cochin University of Science and Technology

Article

Keywords:

Posted Date: November 26th, 2026

DOI: https://doi.org/10.21203/rs.3.rs-11586094/v1

License: This work is licensed under a Creative Commons Attribution 4.0 International License.
Read Full License

Additional Declarations: No competing interests reported.

Abstract

Microbial fuel cell (MFC) performance depends on both the anode material and the way the inoculum is delivered to it, yet the two are rarely varied together. Here, six *Chlorella vulgaris*-fed MFCs were operated for 25 fed-batch cycles in a two-factor design combining two anode materials, carbon felt and stainless steel, with three inoculation regimes: suspended acclimatized sludge, sludge immobilized in calcium alginate beads, and beads additionally amended with powdered activated carbon. Carbon felt outperformed stainless steel at every level of inoculation, and within each anode material the carbon powder-amended beads gave the highest output. The best configuration (MFC-CBC) reached 230.7 ± 2.0 mV, a maximum power density of 65.2 ± 23.2 mW m^{-2} and a maximum current density of 313 ± 34 mA m^{-2}, removing 74.5 ± 2.8% of the influent chemical oxygen demand at a coulombic efficiency of 30.2 ± 1.1%, a 2.3-fold gain in power density over the suspended-sludge control. Amplicon sequencing of the two carbon powder-amended biofilms showed a higher *Proteobacteria*-to-*Firmicutes* ratio and more *Geobacter* on carbon felt, whereas predicted extracellular electron transfer gene abundances were comparable between the two anodes.

Introduction

Microbial fuel cells (MFCs) are bioelectrochemical systems that exploit the metabolic activity of microorganisms to convert chemical energy stored in organic substrates into electrical energy. They have been studied widely for decentralised power generation, wastewater treatment and resource recovery because they can remove chemical oxygen demand (COD) and produce electricity simultaneously[1]. Wider application is nevertheless limited by low and unstable power densities, biomass washout, slow start-up and limited long-term operational stability. One promising route around these constraints is immobilization of the microbial inoculum, in which wastewater or activated sludge is retained within or upon a support matrix to improve cell retention, biofilm formation and electron transfer to the electrode[2].

Waste activated sludge is an attractive inoculum because it is abundant, inexpensive and already contains a complex electroactive community able to oxidise organic matter and respire an anode. Suspended sludge, however, attaches poorly to electrode surfaces, is washed out in the effluent, forms biofilms inconsistently, and loses electrogenic populations during hydraulic disturbance. Immobilization addresses these problems by trapping cells in a physical matrix, raising microbial cell density near the electrode interface, stabilising the biofilm and reducing washout; these effects commonly translate into faster start-up, higher coulombic efficiency and steadier power output[3,4]. Immobilization also organises microorganisms and substrate in space, buffers cells against shear and toxic shock, and supports pre-colonisation or bioaugmentation strategies that shorten reactor maturation. Recent reviews identify it as a practical way to reduce both sludge production and reactor footprint while improving treatment performance when coupled to MFCs[5,6].

The choice of matrix governs mass transfer, mechanical strength, microbial viability and electron transfer. Sodium alginate and agar are used widely for entrapment because they gel under mild conditions that preserve viability, and Ca^{2+}-crosslinked alginate beads are simple to prepare and have been applied both to activated sludge and to defined electrogenic strains. Pure alginate is, however, mechanically weak and electrically insulating, limitations that can be mitigated by embedding conductive particles such as activated carbon or biochar in the gel[7].

Substrate cost is a second constraint on practical deployment. Much MFC research uses defined organic compounds such as acetate, glucose, pentoses, phenol, cysteine and alcohols, which support reproducible microbial growth but are too expensive for long-term commercial operation. Microalgal biomass is an alternative feedstock that is abundant in eutrophic water bodies and couples energy recovery to remediation[8]. It is also compositionally well suited to fermentative and electrogenic consortia, with high protein (~ 32%) and carbohydrate (~ 51%) contents that are readily hydrolysed once the cell wall is disrupted[9].

Anode material determines the area available for colonisation, the electrical path from cell to circuit, and the biocompatibility of the interface. Carbon-based anodes dominate the field and include graphite rods, graphite fibre, carbon felt, carbon cloth and carbon paper, and surface modification of these materials has repeatedly been shown to alter power output[10]. Chaudhuri and Lovley reported that graphite rods were less efficient than carbon felt anodes and attributed the difference to the greater biofilm area supported by the felt and the correspondingly larger bacterial–anode contact[11]. Stainless steel, by contrast, is cheap, mechanically robust and highly conductive, but presents a smooth, essentially two-dimensional surface that is less readily colonised.

These two levers, the anode material and the physical form in which the inoculum is presented to it, are usually studied separately, so their relative contributions and any interaction between them remain poorly resolved. Immobilization is also commonly credited with improving electron transfer when the evidence supports only improved biomass retention, and the conductivity added by carbon amendment is rarely separated from the retention effect. The present study therefore addresses three questions. First, how much of the performance gain from a carbon powder-amended immobilized inoculum is retained when the anode is changed from a porous carbon felt to a planar stainless steel? Second, do the resulting biofilms differ in composition in a way that tracks the electrochemical performance? Third, can the improvement be attributed specifically to enhanced extracellular electron transfer, or is it better explained by biomass retention and interfacial area? To answer these, six MFCs spanning a two-factor design of two anode materials and three inoculation regimes were operated in parallel under identical conditions on ultrasonicated *Chlorella vulgaris* biomass, and the anodic biofilms of the two carbon powder-amended reactors were characterised by 16S rRNA gene amplicon sequencing with predictive functional profiling and community-scale metabolic modelling.

Results

Voltage generation

Voltage output rose progressively in all six reactors across the 25 operational cycles, consistent with continuing biofilm colonisation and increasing electroactive microbial activity (Fig. 1a). Among the configurations tested, MFC-CBC consistently delivered the highest output, reaching 230.74 ± 2.0 mV by cycle 25. MFC-SBC was second at 179.67 ± 2.0 mV, followed by MFC-CB (145.39 ± 2.0 mV), MFC-CS (134.47 ± 2.0 mV), MFC-SB (124.32 ± 2.0 mV) and MFC-SS (123.54 ± 2.0 mV). The ordering places both carbon powder-amended reactors above every other configuration and places each carbon felt reactor above its stainless steel counterpart at the same level of inoculation.

One-way ANOVA on the cycle-25 voltages indicated a significant effect of reactor configuration ($F_{5,12}$ = 1178.64, $p < 0.001$). Tukey's post-hoc test separated MFC-CBC from all other configurations ($p < 0.05$). The two poorest configurations, MFC-SB and MFC-SS, differed by less than 1 mV with a reported standard deviation of 2.0 mV and were not separated by the post-hoc test; all other pairwise contrasts were significant at $p < 0.05$.

Voltage had not plateaued in any reactor by cycle 25. The near-linear rise over the full 100-day operating period indicates that none of the systems had reached a steady state within the experiment, and the values reported above are therefore end-of-experiment rather than asymptotic outputs.

COD removal and coulombic efficiency

COD removal and coulombic efficiency (CE) increased in every reactor over successive cycles and preserved the same ranking as the voltage data (Fig. 1b,c). In MFC-CBC, COD removal rose from 22.76 ± 2.58% at cycle 5 to 74.51 ± 2.84% at cycle 25, while CE rose from 2.37 ± 0.33% to 30.21 ± 1.05% over the same interval. MFC-SBC was again second, reaching 68.14 ± 2.01% COD removal and 22.41 ± 1.21% CE at cycle 25, followed by MFC-CB (65.14 ± 2.10%; 17.90 ± 1.23%), MFC-CS (60.41 ± 1.54%; 14.54 ± 1.05%), MFC-SB (56.74 ± 1.57%; 12.65 ± 0.80%) and MFC-SS (53.24 ± 0.95%; 11.87 ± 0.90%).

One-way ANOVA at cycle 25 confirmed a significant effect of reactor configuration on both COD removal ($F_{5,12}$ = 52.94, $p < 0.001$) and CE ($F_{5,12}$ = 138.99, $p < 0.001$). Across reactors, higher COD removal was accompanied by higher CE, indicating that the configurations that degraded more substrate also recovered a larger fraction of the available electrons as current rather than losing them to competing sinks.

Polarization and power density

Polarization behaviour was conventional in all six reactors: cell voltage fell progressively as current density increased, and power density passed through a maximum before declining under the combined influence of activation, ohmic and mass-transfer losses (Fig. 1d). MFC-CBC gave the highest maximum

power density, 65.16 ± 23.20 mW m^{-2}, and the highest maximum current density, 312.72 ± 33.67 mA m^{-2}, the latter reached at the low-resistance end of the sweep rather than at the power maximum. MFC-SBC and MFC-CB were intermediate at 47.91 ± 5.54 and 44.79 ± 5.13 mW m^{-2}, respectively, while MFC-CS, MFC-SB and MFC-SS reached 28.46 ± 1.23, 25.03 ± 0.74 and 22.89 ± 0.80 mW m^{-2}. One-way ANOVA indicated a significant effect of configuration on maximum power density ($F = 10.62$, $p < 0.001$).

Internal resistance was estimated for each reactor from the slope of its polarization curve over a fixed central window spanning 20–80% of the current range (Table 2). It increased monotonically as performance fell, from 267 Ω in MFC-CBC to 676 Ω in MFC-SS, so that the ranking of internal resistance is the inverse of the ranking of power output. The linear fit was good for five of the six reactors (R^2 = 0.957–0.996) but poorer for MFC-SS (R^2 = 0.87), whose polarization curve departs from ohmic behaviour and is therefore limited by activation and mass-transfer losses rather than by ohmic resistance alone. The standard deviation on the maximum power density of MFC-CBC (± 23.20 mW m^{-2}, 36% of the mean) is considerably larger than that of any other reactor and reflects substantial replicate-to-replicate variability in the region of peak power; the corresponding values for the other five configurations varied by less than 5% of their means.

All power and current densities are normalised to the projected geometric area of the anode (77 cm^2).

Table 2
Parameters derived from the polarization curves of the six reactors. Internal resistance is the slope of the voltage–current curve over 20–80% of the current range; R^2 is the coefficient of determination of that linear fit. All densities are normalised to the projected anode area (77 cm^2).

Reactor	V at 10 kΩ (mV)	R_{int} (Ω)	R^2	P_{max} (mW m^{-2})	j_{max} (mA m^{-2})
MFC-CBC	747	267	0.957	65.16	313.0
MFC-SBC	692	366	0.983	47.91	251.2
MFC-CB	661	542	0.988	44.79	185.7
MFC-CS	601	515	0.996	28.46	176.0
MFC-SB	548	569	0.981	25.03	163.9
MFC-SS	533	676	0.867	22.89	141.9

Voltammetric characterisation

Cyclic voltammograms recorded between − 1.0 and + 1.0 V at 10 mV s^{-1} showed oxidation and reduction features in all six reactors, consistent with the presence of electroactive biofilms (Fig. 2a). The magnitude and shape of the voltammograms varied with reactor configuration. MFC-CBC produced the largest current response, approximately 33.2 mA at + 1.0 V, and enclosed the largest voltammetric area;

MFC-SBC was second, followed by MFC-CB, MFC-SB and MFC-CS, with MFC-SS giving the smallest response across the scanned range. Oxidation features in the voltammograms of MFC-CBC and MFC-SBC are consistent with the presence of redox-active species such as outer-membrane cytochromes, although the two-electrode configuration used here does not allow the responsible couples to be assigned to defined formal potentials.

Linear sweep voltammetry over the same range gave the same ranking (Fig. 2b). MFC-CBC reached approximately 21.8 mA at + 1.0 V, followed by MFC-SBC (18.7 mA), MFC-CB (18.5 mA) and MFC-CS (18.3 mA), while MFC-SB and MFC-SS reached only about 14.8 and 12.2 mA. MFC-CBC and MFC-SBC also showed steeper current–potential slopes in the mid-range of the sweep.

Because both experiments were performed in a two-electrode cell, the abscissa in Fig. 2 is the applied cell voltage and not an anode potential referred to a reference electrode. The currents quoted at + 1.0 V lie far outside the 0.12–0.23 V range at which the reactors actually operated, and at this applied cell voltage water electrolysis and other background faradaic processes are expected to contribute to the measured current. These values are therefore reported as a relative comparison between identically configured cells rather than as a measure of biofilm turnover under operating conditions.

Anodic biofilm community structure

Both reactors received the same carbon powder-amended immobilized inoculum (Fig. 3a), so this comparison isolates the effect of the anode material. Biofilms recovered from the carbon felt anode of MFC-CBC (designated CF-AC) and the stainless steel anode of MFC-SBC (SS-AC) were sequenced to compare community composition between the two anode materials at a constant inoculum. *Firmicutes*, *Proteobacteria* and *Bacteroidota* dominated both biofilms, together accounting for 85.8% of prokaryotic reads in CF-AC and 83.4% in SS-AC (Fig. 3b). *Proteobacteria* were relatively more abundant in CF-AC (29.6% against 24.2%), as were *Bacteroidota* (22.3% against 16.9%), whereas *Firmicutes* were relatively more abundant in SS-AC (42.4% against 33.9%). *Actinobacteriota*, *Desulfobacterota* and *Chloroflexi* were each present at between 1.6% and 4.6%, with a further 3.0% in CF-AC and 5.5% in SS-AC distributed among phyla below 1% relative abundance.

The *Proteobacteria*-to-*Firmicutes* (P/F) ratio was higher in CF-AC (0.87) than in SS-AC (0.57) (Fig. 3c); because both phyla are rescaled identically, this ratio is unaffected by the exclusion of the off-target reads. Most of the exoelectrogens characterised to date, including *Geobacter*, *Desulfovibrio* and *Pseudomonas*, fall within the *Proteobacteria*[12], whereas the electroactive members of the *Firmicutes* generally rely on secreted mediators rather than direct contact-based transfer.

Differential abundance analysis of the 30 most abundant genera (Fig. 3d) showed *Acidovorax*, *Bacteroides*, *Lentimicrobium*, *Azoarcus*, *Sphingopyxis*, *Anaerovorax* and *Desulfovibrio* at higher relative abundance in CF-AC, and *Acetoanaerobium*, *Thauera*, *Microbacterium*, *Pseudomonas*, *Syntrophomonas*, *Bifidobacterium* and *Blautia* at higher relative abundance in SS-AC.

Among the genera with recognised extracellular electron transfer (EET) capability (Fig. 3e), *Pseudomonas* was the most abundant in both biofilms and was relatively more abundant in SS-AC (≈ 1.06%) than in CF-AC (≈ 0.85%). *Geobacter*, which transfers electrons directly via conductive pili and outer-membrane cytochromes, was approximately three times more abundant in CF-AC (≈ 0.29%) than in SS-AC (≈ 0.10%). *Clostridium sensu stricto* members were present in both but partitioned differently between clades, and *Aeromonas* was comparably abundant on both anodes. *Shewanella* and other *Geobacteraceae* were detected at low abundance.

Sequencing was performed on a single pooled biofilm sample per anode material (920,794 reads for CF-AC and 838,350 for SS-AC). The compositional differences reported in this section are therefore descriptive and were not tested statistically.

Predicted functional and metabolic profiles

PICRUSt2 predicted the presence of genes associated with EET in both biofilms, including those encoding the cytochromes CymA, MtrA, MtrB, MtrC and OmcE and the conductive pilin PilA (Fig. 4a). Predicted abundances were closely similar between the two anodes and, where they differed, did not favour the better-performing carbon felt biofilm: *mtrC* was the most abundant marker in both communities at 0.061% (CF-AC) and 0.063% (SS-AC), *cymA* was predicted at 0.014% in CF-AC against 0.019% in SS-AC, and *mtrA*, *mtrB*, *omcE* and *pilA* were comparable between the two. These predictions therefore provide no evidence of preferential enrichment of EET machinery on the carbon felt anode.

The 15 most abundant predicted KEGG pathways were likewise shared between the two biofilms and were dominated by amino acid biosynthesis, cofactor metabolism, fatty acid synthesis, nucleotide biosynthesis and central carbon metabolism (Fig. 4b). CF-AC showed a marginally larger representation of several biosynthetic and energy-related pathways.

Community-scale metabolic modelling with MICOM predicted a higher community growth rate for CF-AC (0.0161 h^{-1}) than for SS-AC (0.0072 h^{-1}) (Fig. 4c). At the level of individual taxa, the model predicted higher growth rates in CF-AC for *Pseudomonas*, *Desulfovibrio*, *Acinetobacter*, *Bacteroides* and several fermentative genera, while fewer taxa were predicted to grow faster in SS-AC (Fig. 4d).

All values in Fig. 4 are model inferences derived from 16S rRNA gene amplicon data. They are predictions of genomic potential and simulated flux, not measurements of gene expression, enzyme activity or metabolic flux, and they inherit the single-sample limitation of the underlying sequencing.

Discussion

Both factors contribute, and they are separable for the electrochemical data

The two-factor design allows the contributions of anode material and inoculation regime to be distinguished for the electrochemical and treatment data, because all six reactors were operated in parallel under identical conditions and each anode material was tested at all three levels of inoculation. Two consistent effects emerge. At every level of inoculation, the carbon felt reactor outperformed its stainless steel counterpart, and within each anode material, performance increased from suspended sludge to immobilized sludge to carbon powder-amended immobilized sludge. The two effects are additive in direction and the best configuration combines both.

The magnitude of the inoculation effect is modest when expressed against the appropriate control. On carbon felt, the carbon powder-amended beads raised maximum power density from 28.46 ± 1.23 mW m^{-2} (MFC-CS, suspended sludge) to 65.16 ± 23.20 mW m^{-2} (MFC-CBC), a 2.29-fold increase, and raised coulombic efficiency from 14.54 ± 1.05% to 30.21 ± 1.05%. The direction and scale of these gains are consistent with earlier reports in which conductive particles were embedded in alginate or sludge was retained in a gel matrix[4,7].

Retention and interfacial area explain the data better than enhanced electron transfer

It is tempting to attribute the improvement to faster extracellular electron transfer, and the voltammetric data are superficially consistent with that reading. The sequencing and functional data do not support it. Predicted abundances of the EET marker genes were comparable between the two anodes, and the two markers that differed most, *mtrC* and *cymA*, were marginally higher in the poorer-performing stainless steel biofilm (Fig. 4a). The genetic capacity for extracellular electron transfer was therefore present in both communities at similar predicted levels, and the difference in performance cannot be ascribed to its differential enrichment.

A more parsimonious explanation is that the carbon felt anode and the carbon powder-amended matrix both increase the quantity of catalytically engaged biomass in electrical contact with the circuit, rather than increasing the per-cell rate of electron transfer. Carbon felt presents a porous, high-area, conductive three-dimensional scaffold, whereas stainless steel presents a smooth, essentially planar surface; the former supports more biofilm per unit projected area and shortens the mean distance from a cell to a conductive surface. Powdered activated carbon dispersed through the alginate extends conductive material into the bead interior, which would otherwise be electrically isolated, and the beads themselves retain biomass that would be washed out in the suspended-sludge controls. On this reading, the higher *Geobacter* abundance and higher P/F ratio on carbon felt (Fig. 3c,e) are a consequence of a more favourable colonisable interface rather than evidence of a distinct electron transfer mechanism.

This interpretation also sets a limit on what the voltammetry can establish. A larger enclosed voltammetric area and a higher current are consistent with a greater quantity of electroactive and capacitive material at the interface, but they do not by themselves demonstrate faster anodic electron

transfer kinetics, and they cannot be used to infer electroactive biomass quantitatively in the absence of an independent biomass measurement.

Confounding between electrode material and electrochemical response

A further caution applies to the voltammetric comparison in Fig. 2. The six cells differ not only in their biofilms but in the material, surface area and roughness of the anode, and in the presence or absence of powdered activated carbon in the anodic compartment. Both carbon felt and activated carbon are themselves capacitive and electrochemically active, so part of the difference in current response and enclosed area between configurations is attributable to the electrode and carbon loading rather than to microbial activity. Abiotic controls, in which the same electrode and bead configurations are assembled without an inoculum, were not run in this study and would be required to apportion the response between biotic and abiotic contributions. The voltammetric data are therefore reported here as a comparison between complete assembled cells, and the attribution of the differences to microbial activity alone is not supported.

Cathode limitation and the validity of the anodic comparison

The cathode in all six reactors was catalyst-free carbon felt operating on aerated distilled water. Distilled water has a low ionic conductivity and the cathode carried no oxygen reduction catalyst, so the cathodic reaction is expected to be slow and to limit the absolute output of every reactor. Two consequences follow. First, absolute power and current densities obtained here should not be compared directly with systems that use buffered catholytes or catalysed air cathodes, and they understate what the same anodes could deliver in a better-balanced cell. Second, and more usefully, because the cathode, catholyte, membrane, external resistance and feeding regime were identical across all six reactors, the cathodic contribution is a common offset and the differences between reactors remain attributable to the anodic compartment. The comparison between configurations is thus internally valid even though the absolute values are cathode-limited. Deliberate cathode limitation also compresses the dynamic range of the measurement, which may explain why the ranking of configurations was preserved across every metric while the absolute separations remained small.

The near-linear voltage trajectory in Fig. 1a is consistent with this picture. None of the reactors reached a plateau within 25 cycles, so the experiment characterises the colonisation phase rather than a mature steady state, and the reported cycle-25 values should be read as the output after 100 days of operation rather than as stable performance.

Role of the algal substrate

Chlorella vulgaris biomass was used here as a low-cost, renewable feedstock whose protein and carbohydrate fractions are readily hydrolysed after ultrasonication. The present design does not isolate the contribution of the algal substrate itself, because no reactor was run on a defined substrate such as

acetate under otherwise identical conditions. What the data do show is that a particulate algal feedstock supports coulombic efficiencies up to 30% in an immobilized-sludge MFC, and that the hydrolytic and fermentative genera enriched on both anodes, including *Bacteroides*, *Lentimicrobium*, *Clostridium sensu stricto* and *Syntrophomonas*, are consistent with a two-step conversion in which complex algal polymers are fermented to short-chain acids that are subsequently respired by electrogens. Confirming that syntrophy would require measurement of volatile fatty acid intermediates, which was not performed.

Normalization and comparison with reported systems

Power and current densities here are normalised to the projected geometric area of the anode (77 cm^2). For carbon felt this substantially understates the true accessible surface area, since the felt is a three-dimensional fibrous matrix whose specific surface area exceeds its projected area by orders of magnitude, while for the planar stainless steel anode the projected area is a much closer approximation. Normalisation by projected area therefore flatters carbon felt relative to stainless steel, and comparisons with literature values normalised to real surface area, to total electrode mass, or to anode chamber volume are not equivalent. Within this study the normalisation is applied identically to all six reactors and the comparison between them is unaffected; between studies, the values should be treated as indicative only. Reporting on more than one basis, and measuring the actual surface area of the felt, would make future comparisons more robust.

In absolute terms the maximum power density obtained here is modest compared with acetate-fed systems using catalysed cathodes. The relevant context is that this output was obtained from a complex particulate algal substrate in a membrane-separated two-chamber reactor with an uncatalysed air cathode and a fixed 100 Ω external load. It should also be noted that the energy required for cathode aeration and for ultrasonic pretreatment of the biomass was not measured and is not included in any energy balance; on current evidence the net energy balance of the system as operated is unlikely to be positive, and the results are therefore presented as a comparison of anode and inoculum configurations rather than as a demonstration of practical energy recovery.

Limitations

Several limitations qualify the conclusions. The electrochemical characterisation used a two-electrode configuration, so the potentials in Fig. 2 are cell voltages and cannot be assigned to the anode on an absolute scale; three-electrode measurements against a reference electrode would be needed to resolve the redox couples responsible for the oxidation features, and to compare currents at operationally relevant anode potentials rather than at ± 1.0 V. Sequencing was performed on one pooled biofilm sample per anode material, so all compositional and predicted functional differences between CF-AC and SS-AC are descriptive and cannot be tested statistically; they also compare two anode materials at a fixed inoculum and therefore do not address the effect of the inoculation regime itself, which remains uncharacterised microbiologically. PICRUSt2 and MICOM outputs are inferences from marker-gene data, and the MICOM growth rates in particular are simulated quantities that should not be read as evidence of reduced toxicity or of demonstrated syntrophy. Absolute microbial biomass in the anode

compartment was not quantified, so relative abundances cannot be converted into absolute population sizes and the central interpretation advanced here, that more catalytically engaged biomass rather than faster per-cell transfer explains the result, remains to be tested directly. Finally, the reactors were operated for 25 fed-batch cycles without reaching steady state, and longer operation would be required to establish whether the alginate matrix retains mechanical integrity and whether the advantage of the immobilized systems is sustained.

Conclusions

Six *Chlorella vulgaris*-fed microbial fuel cells spanning two anode materials and three inoculation regimes were compared under identical conditions. Carbon felt outperformed stainless steel at every level of inoculation, and carbon powder-amended immobilized sludge outperformed both plain immobilized sludge and suspended sludge on both anode materials. The best configuration, MFC-CBC, reached 230.74 ± 2.0 mV, a maximum power density of 65.16 ± 23.20 mW m^{-2} and a current density of 312.72 ± 33.67 mA m^{-2}, and removed 74.51 ± 2.84% of the influent COD at a coulombic efficiency of 30.21 ± 1.05% by cycle 25, a 2.29-fold improvement in power density over the suspended-sludge control on the same anode.

Amplicon sequencing of the two carbon powder-amended biofilms showed a higher *Proteobacteria*-to-*Firmicutes* ratio and a threefold higher relative abundance of *Geobacter* on carbon felt, while predicted extracellular electron transfer gene abundances were comparable between the two anodes. The combined evidence favours an interpretation in which the conductive porous anode and the carbon-amended bead matrix increase the amount of biomass held in electrical contact with the circuit, rather than one in which the per-cell rate of extracellular electron transfer is enhanced. Testing that interpretation directly will require quantification of anodic biomass, abiotic electrode controls, three-electrode characterisation at operationally relevant potentials, and replicated sequencing across all six configurations.

Methods

MFC construction and operation

Six dual-chamber MFC configurations were constructed and operated in triplicate at 25 ± 2°C. The configurations combined two anode materials with three inoculation regimes and are summarised in Table 1. Carbon felt served as the cathode in all six reactors; the anode was carbon felt in MFC-CS, MFC-CB and MFC-CBC and stainless steel in MFC-SS, MFC-SB and MFC-SBC. The inoculum was suspended acclimatized sludge in MFC-CS and MFC-SS, sludge immobilized in calcium alginate beads in MFC-CB and MFC-SB, and powdered activated carbon-amended immobilized sludge beads in MFC-CBC and MFC-SBC.

Table 1
The six microbial fuel cell configurations compared in this study.

Reactor	Anode	Cathode	Inoculum
MFC-CS	Carbon felt	Carbon felt	Acclimatized sludge (suspended)
MFC-CB	Carbon felt	Carbon felt	Sludge immobilized in calcium alginate beads
MFC-CBC	Carbon felt	Carbon felt	Carbon powder-amended immobilized sludge beads
MFC-SS	Stainless steel	Carbon felt	Acclimatized sludge (suspended)
MFC-SB	Stainless steel	Carbon felt	Sludge immobilized in calcium alginate beads
MFC-SBC	Stainless steel	Carbon felt	Carbon powder-amended immobilized sludge beads

Projected anode area 77 cm^2; cathode area 104 cm^2; external resistance 100 Ω; 0.2 cm clayware proton exchange membrane; substrate ultrasonicated *Chlorella vulgaris* biomass at 3000 mg L^{-1}; all reactors operated in fed-batch mode at 25 ± 2°C in triplicate (n = 3).

The anodic chamber had a working volume of 150 mL excluding headspace, as in the dual-chamber clayware reactors used previously by this group[13]. The projected geometric area of the anode was 77 cm^2 and that of the cathode 104 cm^2. The chambers were separated by a 0.2 cm clayware proton exchange membrane and the electrodes connected through a fixed 100 Ω external resistance. The catholyte was distilled water, aerated continuously with an air pump to sustain the oxygen reduction reaction. No cathode catalyst was used.

Substrate preparation

Chlorella vulgaris was obtained from the Central Marine Fisheries Research Institute (CMFRI), Kochi, India and maintained by successive subculturing in sterilised F/2 medium. Cultures were harvested in late stationary phase, washed with distilled water, sun-dried to constant weight and ground to a fine powder.

Dried biomass was suspended in growth medium at 3000 mg L^{-1} and ultrasonicated at 20 kHz for 5 min to disrupt cells and release intracellular organic matter. The resulting slurry was used as the anodic feed in all configurations. The initial COD of the prepared feed was 3000 mg L^{-1}, which was taken as the baseline for COD removal and coulombic efficiency calculations.

The growth medium contained, per litre: KH_2PO_4 (5356 mg), $K_2HPO_4{\cdot}3H_2O$ (164 mg), $Na_2HPO_4{\cdot}12H_2O$ (11,867 mg), $MgCl_2{\cdot}6H_2O$ (100 mg), $NaHCO_3$ (1000 mg), $CaCl_2{\cdot}2H_2O$ (66 mg), NH_4Cl (500 mg), $MnSO_4{\cdot}6H_2O$ (15 mg), $FeSO_4{\cdot}7H_2O$ (25 mg), $CuSO_4{\cdot}5H_2O$ (5 mg), $CoCl_2{\cdot}5H_2O$ (0.0125 mg), $NiSO_4$ (32 mg), $ZnCl_2$ (23 mg) and $(NH_4)_6Mo_7O_{24}{\cdot}H_2O$ (14 mg), as described previously[14]. Reactors were operated

in fed-batch mode, with freshly prepared algal medium added to the anodic compartment every four days.

Sludge immobilization

Concentrated sludge was collected from the effluent treatment plant of Extra Weave Pvt. Ltd., Cherthala, Kerala, India, and characterised before use. The sludge had a total suspended solids concentration of 24,000 mg L^{-1}, a volatile suspended solids concentration of 15,000 mg L^{-1} and a pH of 7.5, giving a VSS/TSS ratio of 62.5%.

The sludge was mixed with 4% (w/v) sodium alginate solution under continuous stirring to give a homogeneous sludge–alginate suspension. Half of this suspension was amended with powdered activated carbon (particle size 100 µm, analytical grade, Sisco Research Laboratories) at 1 g per 100 mL of sludge–alginate mixture and mixed thoroughly to ensure uniform distribution. Spherical beads were formed by adding each suspension dropwise into sterile 3% (w/v) $CaCl_2$ and allowed to cure for 2–4 h to complete gelation. Cured beads were washed repeatedly with sterile distilled water or phosphate-buffered saline to remove excess calcium ions and loosely attached biomass, stored at 4°C, and acclimatized in growth medium before use as inoculum[15–17]. A photograph of the beads is shown in Fig. 3a.

Electrochemical analysis

Cell voltage across the external resistor was recorded daily with a digital multimeter (DM-86 HTC), and current was obtained from the same instrument. Polarization curves were obtained once, at the end of the operating period (cycle 25) when the cell voltage was stable, by stepping the external resistance from 10,000 Ω down to 5 Ω and allowing 10 min for stabilisation at each resistance before recording voltage and current. The sweep was begun on the day following anolyte replacement. The power produced during routine operation at the fixed 100 Ω load is distinguished throughout from the maximum power density obtained from the polarization curves, the two being separate measurements made under different external loads. Internal resistance was estimated from the slope of the resulting polarization curves over a fixed window spanning 20–80% of the current range, identical for all reactors. Voltage and power were averaged across the three replicate reactors independently, so the product of the mean voltage and the mean current density at a given point does not in general equal the mean power density at that point.

Cyclic voltammetry (CV) and linear sweep voltammetry (LSV) were performed with a µStat-i 400s potentiostat/galvanostat/impedance analyser over an applied cell voltage range of − 1.0 to + 1.0 V at a scan rate of 10 mV s^{-1}, following established practice for bioelectrochemical systems[18,19]. Measurements used a two-electrode configuration with the anode as working electrode and the cathode

as counter electrode; no reference electrode was used, so the abscissa in Fig. 2 is an applied cell voltage rather than an electrode potential.

COD and coulombic efficiency

COD was determined by the standard closed reflux method[20,21]. Coulombic efficiency was calculated as described by Logan[22]:

$$CE\ (\%) = M\ (\int I\ dt) / (F \times b \times \Delta COD \times V) \times 100$$

where M is the molecular weight of oxygen (32 g mol^{-1}), ∫I dt is the total charge passed over the batch cycle, F is the Faraday constant (96,485 C mol^{-1} e^{-}), b is the number of electrons exchanged per mole of oxygen (b = 4), ΔCOD is the change in COD (g L^{-1}) and V is the anode chamber volume (L).

16S rRNA gene amplicon sequencing

Anodic biofilms were recovered from the carbon felt anode of MFC-CBC (CF-AC) and the stainless steel anode of MFC-SBC (SS-AC) once stable performance had been established. Total genomic DNA was extracted and the V3–V4 region of the 16S rRNA gene (product size ≈ 459 bp) amplified using the overhang-adapter primers 16S Amplicon PCR Forward (V3-F) 5'-TCGTCGGCAGCGTCAGATGTGTATAAGAGACAGCCTACGGGNGGCWGCAG-3' and 16S Amplicon PCR Reverse (V4-R) 5'-GTCTCGTGGGCTCGGAGATGTGTATAAGAGACAGGACTACHVGGGTATCTAATCC-3'. Libraries were sequenced on an Illumina MiSeq platform using a PE300 kit, yielding 920,794 reads for CF-AC and 838,350 reads for SS-AC. Sequence processing, quality filtering, taxonomic assignment against the SILVA 138 99% naïve Bayes classifier[23] and diversity analyses were performed in QIIME 2[24]. One pooled biofilm sample was sequenced per anode material. A minority of reads, 8.5% in CF-AC and 11.2% in SS-AC, were assigned to the fungal phyla *Ascomycota* and *Basidiomycota*. These cannot be recovered with the bacterial V3–V4 primer set and were therefore treated as off-target amplification or reference-database misassignment and excluded; community composition is reported for the prokaryotic fraction, renormalised to 100%.

Functional prediction and metabolic modelling

Functional potential was predicted with PICRUSt2 (v2.5.2)[25]. Representative sequences were placed into a reference phylogeny using SEPP and gene family abundances inferred by hidden-state prediction, with predicted pathways annotated against the Kyoto Encyclopedia of Genes and Genomes (KEGG) database[26,27]. No KEGG pathway maps or other KEGG imagery were reproduced or adapted; KEGG is used here only as the annotation source for the predicted gene families. Community-scale metabolic modelling was performed with MICOM[28], using genome-scale metabolic reconstructions assigned from

the taxonomic profiles to predict community and taxon-specific growth rates by flux balance analysis. Both outputs are predictions derived from marker-gene data rather than direct measurements.

Statistical analysis

Electrochemical and treatment experiments were performed in triplicate (n = 3) and are reported as mean ± standard deviation. Differences between reactor configurations were assessed by one-way ANOVA followed by Tukey's multiple comparison test, with significance taken at $p < 0.05$[29,30]. Analyses were performed in GraphPad Prism v10 (GraphPad Software, San Diego, CA, USA); data handling and preliminary calculations were performed in Microsoft Excel 2021 (Microsoft Corporation, Redmond, WA, USA). Variance was markedly unequal between configurations for maximum power density, where the standard deviation of MFC-CBC exceeded that of the other reactors by more than an order of magnitude; the corresponding ANOVA is therefore reported as an indication of between-group separation rather than as a formal test, and a variance-corrected or rank-based alternative would be preferable. No statistical analysis was applied to the sequencing data, which comprised one pooled sample per anode material.

Declarations

Additional information of generative AI use.

Claude (Anthropic) to assist with language editing, and checking of the reference list. The authors reviewed, modified and validated all content and take full responsibility for the content and accuracy of the published article.

Competing interests

The authors declare no competing interests.

Author Contribution

A.U. and R.P.P. conceived and designed the study. A.U. performed the experiments, analysed the data, prepared Figures 1–4 and Tables 1 and 2, and wrote the main manuscript text. M.T.N. contributed to the methodology, verified the electrochemical and statistical analyses, revised the figures and tables, and edited the manuscript. M.T.N. and R.P.P. supervised the study and acquired funding. R.P.P. provided resources. All authors reviewed the manuscript.

Acknowledgement

The authors gratefully acknowledge Cochin University of Science and Technology for laboratory access, and the UGC-BSR start-up grant for financial support under UGC order number F.30-566/2021 (BSR) dated 02/12/2024. M.T.N. acknowledges grant RYC2024-049008-I funded by MICIU/AEI/10.13039/501100011033 and by FSE+.

Data Availability

The 16S rRNA gene amplicon sequencing data generated in this study have been deposited in the National Center for Biotechnology Information (NCBI) Sequence Read Archive (SRA) under BioProject accession number PRJNA1556747, with run accession numbers SRR41539871 and SRR41539872. These data are publicly available and may be accessed directly at https://trace.ncbi.nlm.nih.gov/Traces/?view=run_browser&acc=SRR41539871&display=metadata and https://trace.ncbi.nlm.nih.gov/Traces/?view=run_browser&acc=SRR41539872&display=metadata. All other data supporting the findings of this study are available within the article, and the underlying datasets are available from the corresponding authors on reasonable request.

References

1. Wang, J., Ren, K., Zhu, Y., Huang, J. & Liu, S. A review of recent advances in microbial fuel cells: preparation, operation, and application. *BioTech*11, 44 (2022).
2. Jalili, P., Ala, A., Nazari, P., Jalili, B. & Ganji, D. D. A comprehensive review of microbial fuel cells considering materials, methods, structures, and microorganisms. *Heliyon* **10**, e25439 (2024).
3. Ayol, A., Biryol, İ., Taşkan, E. & Hasar, H. Enhanced sludge stabilization coupled with microbial fuel cells (MFCs). *Int. J. Hydrogen Energy*. **46**, 29529–29540 (2020).
4. Yong, Y. et al. Enhancement of coulombic efficiency and salt tolerance in microbial fuel cells by graphite/alginate granules immobilization of *Shewanella oneidensis* MR-1. *Process. Biochem.* **48**, 1947–1951 (2013).
5. Najim, A. A., Radeef, A. Y., al-Doori, I. & Jabbar, Z. H. Immobilization: the promising technique to protect and increase the efficiency of microorganisms to remove contaminants. *J. Chem. Technol. Biotechnol.* **99**, 1707–1733 (2024).
6. Patwardhan, S. B. et al. Microbial fuel cell united with other existing technologies for enhanced power generation and efficient wastewater treatment. *Appl. Sci.* **11**, 10777 (2021).
7. Cheng, L. et al. The performance of microbial fuel cell with sodium alginate and super activated carbon composite gel modified anode. *AMB Express*. **14**, 67 (2024).
8. U, A., Chacko, A., Priyadarshini, M. & Rajesh, P. P. Utilization of *Chlorella vulgaris* biomass in microbial fuel cell as a feed and the study on its degradation pathway. *Water Sci. Technol.* **92**, 1104–1117 (2025).
9. Osman, A. M., Abdurahman, N. H. & Noormazlinah, A. Revolutionizing bioenergy: the microalgae–microbial fuel cell frontier. *Sci. Technol. Energy Transit.* **79**, 91 (2024).

10. Scott, K., Rimbu, G., Katuri, K., Prasad, K. & Head, I. Application of modified carbon anodes in microbial fuel cells. *Process. Saf. Environ. Prot.* **85**, 481–488 (2007).
11. Chaudhuri, S. K. & Lovley, D. R. Electricity generation by direct oxidation of glucose in mediatorless microbial fuel cells. *Nat. Biotechnol.* **21**, 1229–1232 (2003).
12. Logan, B. E., Rossi, R., Ragab, A. & Saikaly, P. E. Electroactive microorganisms in bioelectrochemical systems. *Nat. Rev. Microbiol.* **17**, 307–319 (2019).
13. Chacko, A. et al. Effect of methyl orange dye concentration on decolorization and bioelectricity generation in an earthen membrane cylindrical microbial fuel cell reactor. *Energies* **19**, 5136 (2026).
14. Yang, Z., Guo, R., Xu, X., Fan, X. & Luo, S. Fermentative hydrogen production from lipid-extracted microalgal biomass residues. *Appl. Energy*. **88**, 3468–3472 (2011).
15. Wu, H. S., Zhang, A. Q. & Wang, L. S. Immobilization study of biosorption of heavy metal ions onto activated sludge. *J. Environ. Sci. (China)*. **16**, 640–645 (2004).
16. Bustos-Terrones, Y. A., Bandala, E. R., Moeller-Chávez, G. E. & Bustos-Terrones, V. Enhanced biological wastewater treatment using sodium alginate-immobilized microorganisms in a fluidized bed reactor. *Water Sci. Eng.* **15**, 125–133 (2022).
17. Doria-Serrano, M. C., Ruiz-Treviño, F. A., Ríos-Arciga, C., Hernández-Esparza, M. & Santiago, P. Physical characteristics of poly(vinyl alcohol) and calcium alginate hydrogels for the immobilization of activated sludge. *Biomacromolecules* **2**, 568–574 (2001).
18. Fricke, K., Harnisch, F. & Schröder, U. On the use of cyclic voltammetry for the study of anodic electron transfer in microbial fuel cells. *Energy Environ. Sci.* **1**, 144–147 (2008).
19. Santoro, C., Arbizzani, C., Erable, B. & Ieropoulos, I. Microbial fuel cells: from fundamentals to applications. *J. Power Sources*. **356**, 225–244 (2017).
20. APHA. *Standard Methods for the Examination of Water and Wastewater* 23rd edn (American Public Health Association, 2017).
21. Wang, X. et al. Accelerated start-up of two-chambered microbial fuel cells: effect of anodic positive poised potential. *Electrochim. Acta*. **54**, 1109–1114 (2008).
22. Logan, B. E. *Microbial Fuel Cells* (Wiley, 2008).
23. Quast, C. et al. The SILVA ribosomal RNA gene database project: improved data processing and web-based tools. *Nucleic Acids Res.* **41**, D590–D596 (2013).
24. Bolyen, E. et al. Reproducible, interactive, scalable and extensible microbiome data science using QIIME 2. *Nat. Biotechnol.* **37**, 852–857 (2019).
25. Douglas, G. M. et al. PICRUSt2 for prediction of metagenome functions. *Nat. Biotechnol.* **38**, 685–688 (2020).
26. Kanehisa, M. & Goto, S. K. E. G. G. Kyoto Encyclopedia of Genes and Genomes. *Nucleic Acids Res.* **28**, 27–30 (2000).
27. Kanehisa, M., Sato, Y., Kawashima, M., Furumichi, M. & Tanabe, M. KEGG as a reference resource for gene and protein annotation. *Nucleic Acids Res.* **44**, D457–D462 (2016).

28. Diener, C., Gibbons, S. M. & Resendis-Antonio, O. MICOM: metagenome-scale modeling to infer metabolic interactions in the gut microbial community. *mSystems*5, e00606-19 (2020).
29. Montgomery, D. C. *Design and Analysis of Experiments* 10th edn (Wiley, 2019).
30. Tukey, J. W. Comparing individual means in the analysis of variance. *Biometrics* **5**, 99–114 (1949).

Figures

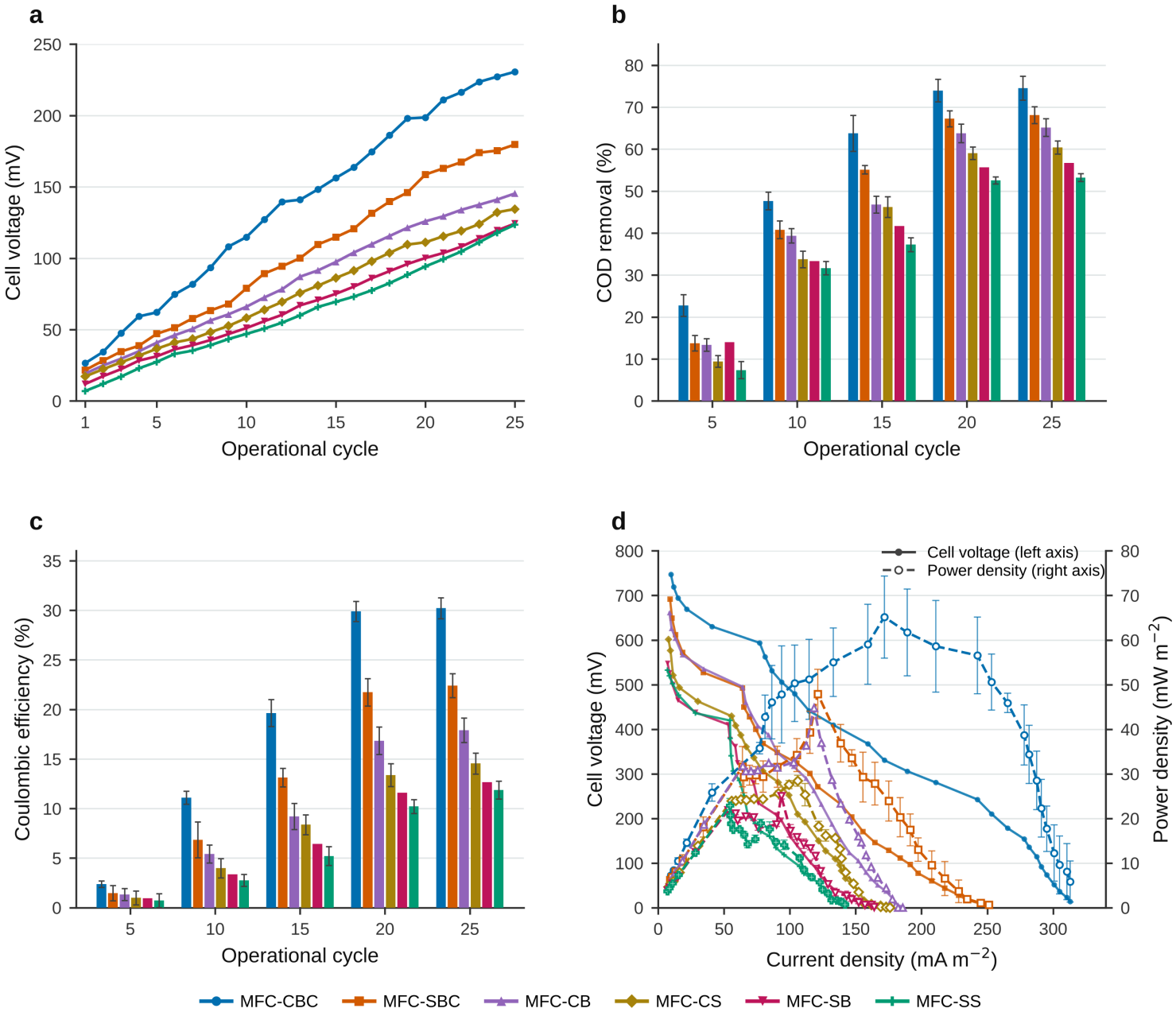

Figure 1

Bioelectrochemical performance of the six MFC configurations. (**a**) Cell voltage over 25 fed-batch cycles. (**b**) COD removal efficiency and (**c**) coulombic efficiency at cycles 5, 10, 15, 20 and 25. (**d**) Polarization (solid symbols, left axis) and power density (open symbols, dashed lines, right axis) curves obtained by

stepping the external resistance from 10,000 to 5 Ω. All current and power densities are normalised to the projected geometric anode area (77 cm^2). Data are mean ± s.d. of three independent reactors (n = 3); error bars in **b** and **c** show s.d. of COD removal and coulombic efficiency, and in **d** the s.d. of power density.

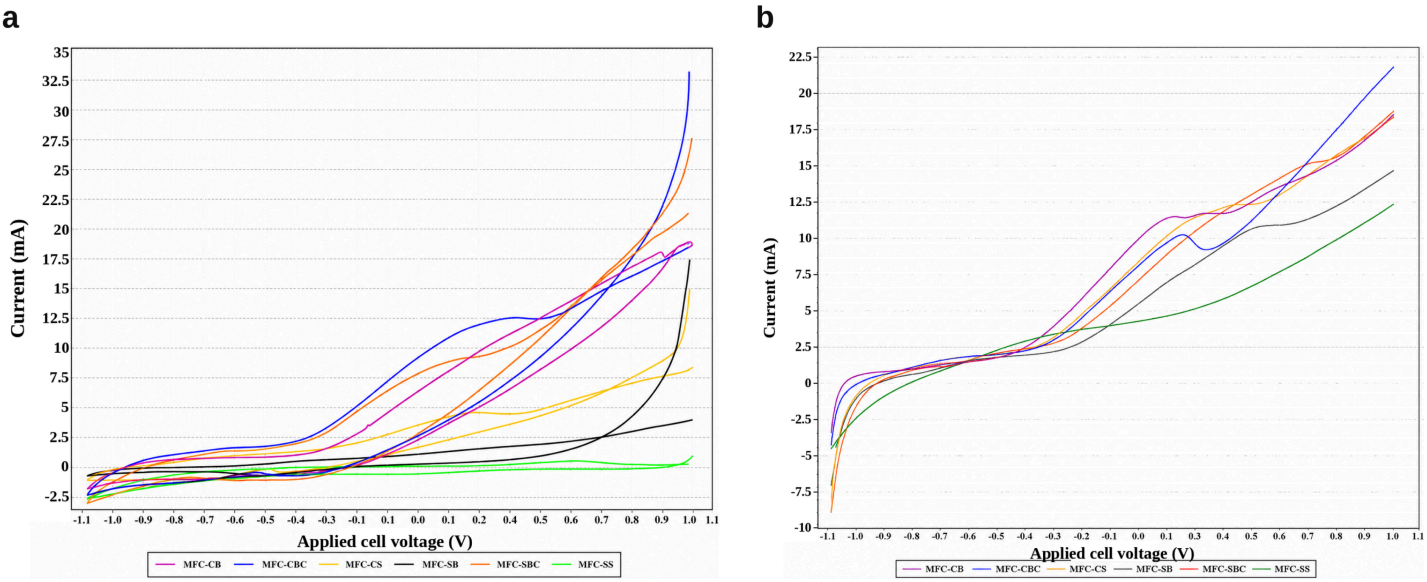

Figure 2

Voltammetric characterisation of the six MFC configurations. (**a**) Cyclic voltammograms and (**b**) linear sweep voltammograms recorded between −1.0 and +1.0 V applied cell voltage at a scan rate of 10 mV s^{-1} in a two-electrode configuration with the anode as working electrode. Because no reference electrode was used, the abscissa is an applied cell voltage and not an anode potential; currents at the extremes of the scanned range include contributions from background faradaic processes. Curves are representative of triplicate experiments (n = 3).

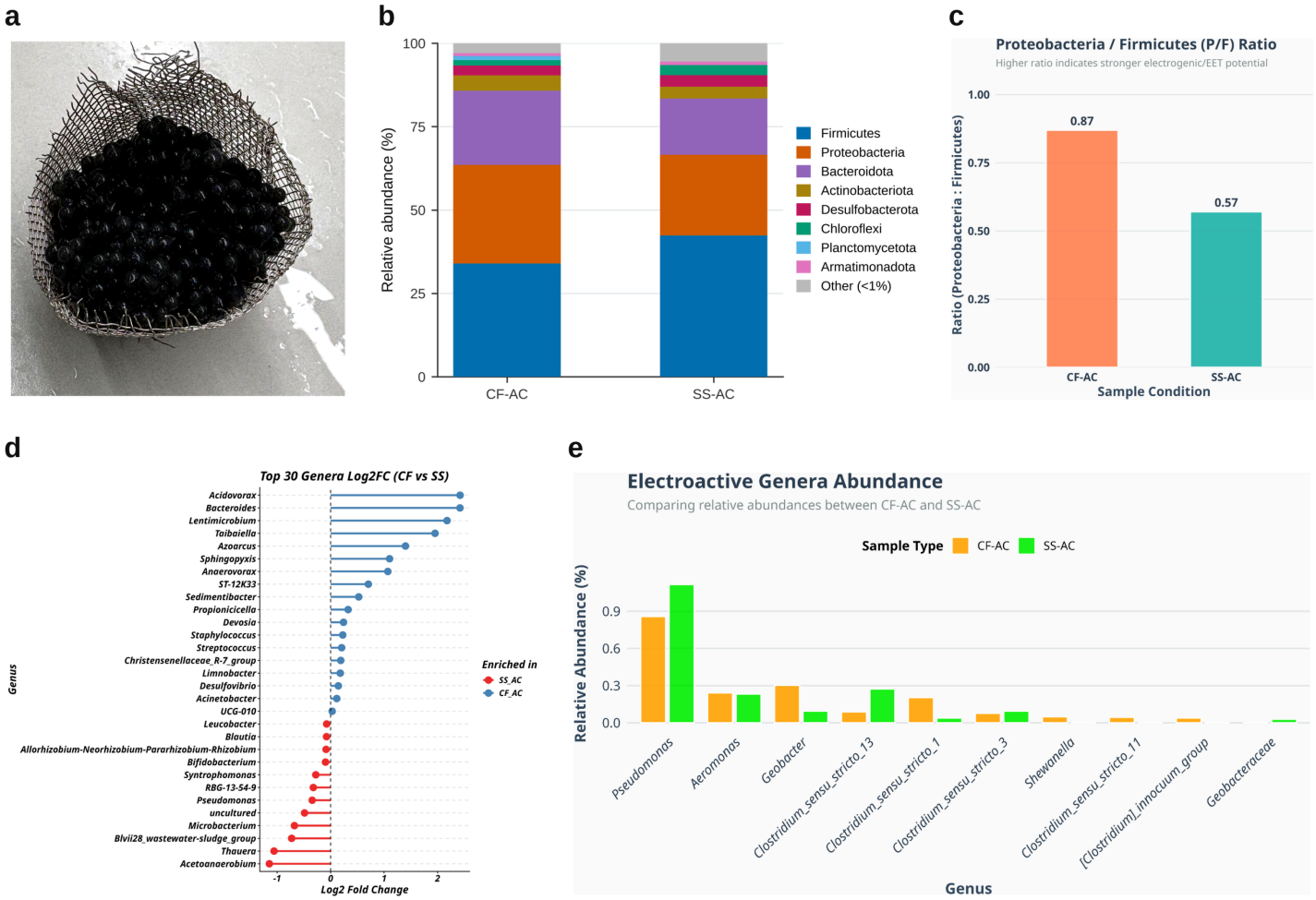

Figure 3

The carbon powder-amended immobilized inoculum and the composition of the anodic biofilms it produced on the two anode materials. (**a**) Carbon powder-amended calcium alginate beads, formed by dropwise addition of a sludge–alginate–powdered activated carbon suspension into 3% (w/v) $CaCl_2$ and cured for 2–4 h; the same bead preparation was used in MFC-CBC and MFC-SBC, so the comparison in **b**–**e** isolates the effect of the anode material. Biofilms were recovered from the carbon felt anode of MFC-CBC (CF-AC) and the stainless steel anode of MFC-SBC (SS-AC). (**b**) Relative abundance of the most abundant prokaryotic phyla, renormalised after exclusion of reads assigned to fungal phyla (Methods); phyla below 1% are pooled. (**c**) *Proteobacteria*-to-*Firmicutes* ratio. (**d**) Differential abundance (log_2 fold change) of the 30 most abundant genera; positive values indicate higher relative abundance in CF-AC. (**e**) Relative abundance of genera with recognised extracellular electron transfer capability. One pooled biofilm sample was sequenced per anode material, so these differences are descriptive and were not tested statistically. The photograph in **a** has been cropped and adjusted uniformly for brightness and contrast; no other processing was applied.



Figure 4

Predicted functional and metabolic profiles of the CF-AC and SS-AC anodic biofilms. (**a**) Predicted relative abundance of extracellular electron transfer gene markers and (**b**) the 15 most abundant predicted KEGG pathways, both inferred with PICRUSt2[25]; pathway annotations derive from the KEGG database[26,27]. (**c**) MICOM-predicted community growth rate and (**d**) MICOM-predicted taxon-specific growth rates of the dominant genera. All values are inferences from 16S rRNA gene amplicon data and are not direct measurements of gene expression or metabolic flux; they derive from a single pooled sample per anode material.